Statistical Analysis of Peptide-Induced Graded and All-or-None Fluxes in Giant Vesicles

Sterling A. Wheaten, Aruna Lakshmanan, and Paulo F. Almeida*
Department of Chemistry and Biochemistry, University of North Carolina Wilmington, Wilmington, North Carolina

ABSTRACT Antimicrobial, cytolytic, and cell-penetrating peptides induce pores or perturbations in phospholipid membranes that result in fluxes of dyes into or out of lipid vesicles. Here we examine the fluxes induced by four of these membrane-active peptides in giant unilamellar vesicles. The type of flux is determined from the modality of the distributions of vesicles as a function of their dye content using the statistical Hartigan dip test. Graded and all-or-none fluxes correspond to unimodal and bimodal distributions, respectively. To understand how these distributions arise, we perform Monte Carlo simulations of peptide-induced dye flux into vesicles using a very simple model. The modality of the distributions depends on the rate constants of pore opening and closing, and dye flux. If the rate constants of pore opening and closing are both much smaller than that of dye flux through the pore, all-or-none influx occurs. However, if one of them, especially the rate constant for pore opening, increases significantly relative to the flux rate constant, the process becomes graded. In the experiments, we find that the flux type is the same in giant and large vesicles, for all peptides except one. But this one exception indicates that the flux type cannot be used to unambiguously predict the mechanism of membrane permeabilization by the peptides.

INTRODUCTION

The molecular mechanism of membrane-active peptides, including antimicrobial, cytolytic, and amphipathic cell-penetrating peptides, has been the subject of much debate, but there is a significant convergence of ideas (1–3). Peptide binding to the membrane surface results in a mass imbalance across the bilayer. Thus strained, the membrane may respond by opening large pores. In some cases, peptide and lipid translocation across the bilayer may occur concomitantly with the formation of pores or defects that allow flux of water and solutes across the membrane. These pores appear to consist of disorganized toroidal holes, lined mostly by lipids but stabilized by peptides, rather than resembling protein channels. Over time, pores may reseal, become smaller, or persist under equilibrium conditions (4,5).

Less progress has been made in the ability to predict those mechanisms. A common method to assess peptide activity is to measure the flux of water-soluble fluorophores (dyes) into or out of lipid vesicles. Most membrane-active peptides belong to one of two types, causing either graded or all-or-none flux across the membrane (1). In graded flux, the vesicle population is homogeneous, that is, the vesicle distribution with respect to their dye content is unimodal. This means that close to the midpoint of the dye flux process, most vesicles contain approximately half of the maximal dye (3). In all-or-none flux, the vesicle population is heterogeneous, that is, the dye content distribution is bimodal, and close to the midpoint, most vesicles are either empty or full of dye (3). Almeida and Pokorny (1) noticed that the Gibbs energy of insertion from the membrane surface into the bilayer interior is $\Delta G^o_{ins} \leq 20$ kcal/mol for most graded peptides, and $\Delta G^o_{ins} \geq 23$ kcal/mol for most all-or-none peptides. Therefore, graded peptides should more easily translocate across the bilayer. All-or-none peptides should accumulate on the surface, because insertion is too costly energetically, until the membrane responds to the strain by forming a large pore, which eventually allows equilibration. In accordance with this hypothesis, they made specific predictions for the mechanism of membrane perturbation by the peptides, based only on the thermodynamics of insertion (1).

Whereas most peptides follow this prediction (1,6), some that have a large ΔG^o_{ins} induce graded flux (7). Thus, graded flux may reflect translocation, but it may also indicate that surface-associated peptides slowly perturb the membrane. If the flux is all-or-none, however, ΔG^o_{ins} appears to be large (1,7). Moreover, the best-studied specifically antimicrobial peptides cause all-or-none flux, as concluded by different research groups using different methods and bilayer systems in the well-known cases of magainin 2 (8–10) and cecropin A (11,12).

Determination of graded and all-or-none types of flux is straightforward in large unilamellar vesicles (LUVs), using the standard 8-aminonaphtalene-1,3,6-trisulfonic acid (ANTS)/p-xylene-bis-pyridinium bromide (DPX) fluorescence requenching assay (13–15). The question arises as to whether the type of flux is the same in giant unilamellar vesicles (GUVs). In the case of magainin 2, the flux is all-or-none in GUVs (9,10), in agreement with the result in LUVs (8). This was shown by comparing dye flux for single GUVs (which occurred abruptly over a short period of time) with flux for the entire population (which occurred smoothly over a much longer period) as a sum of stochastic,

Submitted January 2, 2013, and accepted for publication May 31, 2013.

*Correspondence: almeidap@uncw.edu

Editor: William Wimley.

0006-3495/13/07/0432/12 $2.00

http://dx.doi.org/10.1016/j.bpj.2013.05.055

unsynchronized fluxes of the individual vesicles (9,10). More convincingly, Apellániz et al. (16) demonstrated graded and all-or-none flux by analyzing the distributions of dye content in the GUV population in the presence of a peptide of each type. Understanding the flux type in GUVs is important because experiments with these vesicles provide information about the peptide mechanism that cannot be obtained from LUVs. For example, Lee et al. (17) showed that melittin causes first an increase in vesicle area and then an increase in volume, indicating peptide binding and expansion of the membrane followed by influx of water. This was interpreted as indicating the presence of pores, which persist at equilibrium (17). Other reports contend that melittin pores in GUVs are initially larger and then decrease in size, consistent with a transient perturbation decaying to an equilibrium state in which the membrane recovers much of its original integrity (18,19). Some of these discrepancies may be due to different peptide-to-lipid ratios (P/L) in GUV experiments, where the lipid concentration is especially difficult to control. It is plausible that at higher P/L, more pores persist at equilibrium. Recently, Fuertes et al. (4) showed that the α5 fragment of the proapoptotic protein Bax causes all-or-none flux into GUVs, but the process occurs in two stages, with large transient pores forming first, which later become smaller and persist at equilibrium. Tamba et al. (5) made a similar observation with magainin 2.

The correlations between peptide mechanisms and graded or all-or-none fluxes are intriguing. We posited that the type of flux induced by the peptide into or out of vesicles fundamentally reflects its mechanism of interaction with membranes. Having studied dye flux in LUVs by the ANTS/DPX assay for a large number of peptides (1,6–8,11,20,21), we chose four of those peptides to examine the type of flux in GUVs. Fig. 1 shows the results of the ANTS/DPX assay in LUVs for the four peptides selected. CE-2 and DL-1 (Fig. 1, *A* and *B*) are synthetic variants of cecropin A (11) and δ-lysin (21), respectively, and were chosen because they clearly belong to the graded (CE-2) or all-or-none (DL-1) class in LUVs (7). δ-Lysin and TPW-3, a variant of the cell-penetrating peptide transportan 10 (TP10) (20) (Fig. 1, *C* and *D*), were previously classified as weakly graded (6,21) and may fall in a gray zone between the two types. We sought to determine whether the classifications as graded or all-or-none in LUVs and GUVs coincide, which would be expected if the type of flux reflects a fundamental aspect of the peptide mechanism. Second, we investigated the mechanistic information that could be extracted from this classification. To that end, we performed Monte Carlo simulations of peptide-induced dye influx into vesicles and compared the results with those obtained from experiment. To understand the fundamental process, we kept the model as simple as possible. Graded and all-or-none fluxes were assigned based on the modality of the distributions of vesicle contents using Hartigan's dip test (22).

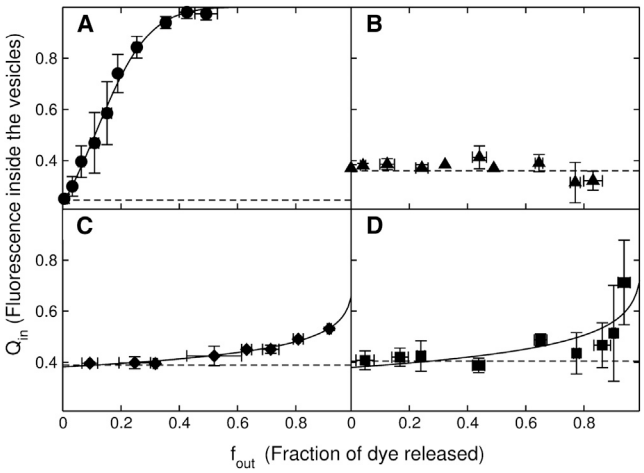

FIGURE 1 ANTS/DPX assay of the peptides examined: (*A*) CE-2, (*B*) DL-1, (*C*) δ-lysin, and (*D*) TPW-3. Data from McKeown et al. (6), Clark et al. (7), and Pokorny and Almeida (21). The measurements were performed in POPC LUVs, except in the case of CE-2, in which LUVs of POPC:1-palmitoyl-2-oleoylphosphatidylglycerol 1:1 were used (7).

We evaluated the results of the simulations by examining the effect of the rates of pore opening and closing relative to the rate of dye influx.

MATERIALS AND METHODS

Chemicals

DL-1 (93% purity) and TPW-3 (95%) were purchased from Bachem (Torrance, CA), and CE-2 (95%) was obtained from New England Peptide (Gardner, MA) or Bachem (>82%). These peptides were from the same batches used in previous studies (6,7). Their identity was ascertained by mass spectrometry, and the purity was determined by high-performance liquid chromatography (HPLC), both provided by the manufacturer. δ-Lysin was a gift from Dr. H. Birkbeck (University of Glasgow). Stock solutions were prepared by dissolving lyophilized peptide in deionized water or water/ethyl alcohol 1:1 (v/v) (AAPER Alcohol and Chemical, Shelbyville, KY). Stock peptide solutions were stored at -80^{o}C and kept on ice during experiments. Peptide concentrations were determined by Trp absorbance at 280 nm. 1-Palmitoyl-2-oleoyl-*sn*-glycero-3-phosphocholine (POPC) and 1,2-dioleoyl-*sn*-glycero-3-phosphoethanolamine-N-lissamine rhodamine B (LRh-DOPE), in chloroform solution, were purchased from Avanti Polar Lipids (Alabaster, AL). Carboxyfluorescein (CF) was purchased from Molecular Probes/Invitrogen (Carlsbad, CA). Bovine serum albumin (BSA, fatty-acid free) was purchased from ICN (Aurora, OH). Lipids and fluorophores were tested by thin-layer chromatography (TLC) and used without further purification. Organic solvents (HPLC/American Chemical Society grade) were purchased from Burdick & Jackson (Muskegon, MI).

Preparation of GUVs

GUVs of POPC, containing 0.1 mol% LRh-DOPE to visualize the membrane, were prepared by electroformation (23). Several other methods were tried (24–28), but the best results were obtained by electroformation (29), with slight modifications to the protocol described by Apellániz et al. (16). Briefly, a 5 μL aliquot of a lipid solution in chloroform (1 mg/mL) was applied onto silver and platinum wire electrodes (1.0 mm diameter, previously cleaned with methanol/dichloromethane 1:1). After

the chloroform evaporated, the electrodes were immersed in a plastic chamber (0.5 mL Eppendorf tube) containing ~ 300 μL 0.1 M sucrose solution, and connected to a sweepable function generator (Global Specialties, New Haven, CT) through the HI output port. Electroformation was performed at 2.4 V, 10 Hz for 2 h, and then at 2 Hz for 30 min (16) using an oscilloscope (Owon HDS1022M hand-held digital oscilloscope and multimeter; Lilliput Technology, City of Industry, CA).

Confocal fluorescence microscopy

Fluorescence microscopy of GUVs was performed with an Olympus Fluoview FV1000 scanning confocal microscope, with excitation by a He-Ne laser at 543 nm for rhodamine, or by an Ar ion laser at 488 nm for CF, reflected by a dichroic mirror (DM405/488/543). The emitted fluorescence was passed through a confocal aperture of 80 μm, and a SDM560 band-pass filter. The samples for microscopy were prepared by adding 10 μL of GUV suspension in 0.1 M sucrose to ~ 240 μL of a solution of 1 μM peptide, 50 μM CF, and 0.1 M glucose, in a culture dish coated with BSA, bound by an O-ring (No. 8; Danco, Waterbury, CT) sealed with silicone high-vacuum grease (Dow Corning, Midland, MI). The exact lipid concentration is not known in this experiment, but from the number and size of vesicles in the images, we estimate it to be ≈30–100 μM. Vesicles with the thinnest membrane contour were deemed to be unilamellar, which has been shown to be a reliable criterion (26), although determining true unilamellarity is beyond the resolution of the fluorescence microscope. Because the sucrose solution is denser than the glucose solution, the GUV aliquot sinks to the bottom of the chamber on the objective plane. The solution is not stirred at this point, and thus the CF and peptide diffuse slowly into the GUV aliquot volume. This means that the fluorescence intensity of the external solution in the field of view increases with time, as does the peptide concentration in contact with the GUVs. This does not alter the dye flux mechanism and gives one more time to focus, decide on the field of view, and optimize instrument settings before collecting data. We optimized the image by scanning in XY mode while adjusting the laser transmissivity and PMT voltage. Then, image scans are collected as a function of time. The final images shown were edited for brightness with the GNU Image Manipulation Program.

Single-vesicle analysis

Quantification of CF fluorescence emission from each vesicle was performed with ImageJ software (16,30). Initially, the vesicle interior was dark and the outside was green, from CF fluorescence. As CF influx occurred, the vesicle interior showed green fluorescence. The degree of filling of each vesicle in a sample was measured as a function of time. The degree of filling is the ratio of the fluorescence intensity in an area inside the GUV to that in an equivalent area outside, near the GUV of interest. The overall midpoint of dye influx (i.e., the point at which the average degree of filling of the GUV sample reaches one-half) is thus located. We then used the image closest to this point in each sample (typically 0.50 ± 0.02) to obtain the distribution of the number of vesicles as a function of their dye content. This analysis was performed for multiple independent samples for each peptide (DL-1, $n = 9$ samples; CE-2, $n = 5$; δ-lysin, $n = 6$; TPW-3, $n = 4$). The data for each peptide at the flux midpoint in each sample were pooled, and the density function and a histogram were generated to show the distribution of degree of filling in the ensemble of all samples. The analysis is independent of time, because the distribution always corresponds to the influx midpoint of each sample. We focused primarily on the population of larger GUVs, with diameter $d \sim 20$–100 μm. The population of smaller GUVs (d<15 μm) reaches the midpoint of influx at a slightly different time, and combining the two populations would blur the determination of the type of influx (graded or all-or-none). For two peptides, CE-2 and TPW-3, we performed separate analyses of small and large GUV populations, and determined their distributions of degree of filling.

Statistical analysis

Qualitatively, if the distribution of vesicles as a function of degree of filling is clearly unimodal or bimodal, as judged by a histogram, the influx is graded or all-or-none, respectively. There are no definite rules regarding the number of bins to be used to display a histogram. Of course, the bin width cannot be smaller than the uncertainty in the abscissa, and the largest bin should contain at least ~ 10 events (31). A more explicit estimate (32) of the optimal number of bins is the smallest integer $>(1 + \log_2 N)$, excluding empty bins, where N is the number of data points. This yields eight bins for $N \approx 90$–120, and nine for $N \approx 100$–160. These are the typical sizes of our experimental and simulation data sets, but some bins in the interval 0–1 are empty. For simplicity and uniformity, rather than varying bin size for each distribution, we display 10 bins for each, which is close to optimal.

Relying on the appearance of the histogram to determine modality, however, is ambiguous, especially when the number of vesicles analyzed is smaller, or the rate constants are such that the type of influx is less well defined. Therefore, to put the assignments of unimodal or bimodal distribution on a rigorous and unbiased basis, we calculated the probability density function of the distribution and performed the Hartigan dip test for modality (22) using the package diptest from R statistical software (33). The density function was calculated directly from the raw data, with the statistically optimal bandwidth (which minimizes the discrepancy between the integrated estimated and true densities), and was independent of the number of bins used for the histogram. The dip test is the standard test to determine whether a distribution is unimodal. Although a few examples of its use have been reported (34,35), it is not well known in the biophysical literature. Therefore, a brief description is justified. The dip test assesses the probability that a given distribution is unimodal by calculating the value of the dip (D) and the associated p-value. The dip statistic measures the difference between the observed distribution and the best unimodal distribution that fits the data. The smaller the dip, the higher is the probability that the distribution is unimodal. The p-value associated with the dip statistic measures the strength of the evidence for rejecting the null hypothesis of unimodality. The smaller the p-value, the less likely it is that the distribution is unimodal. Typically, a p-value <0.05 is considered significant to discard the null hypothesis, and a bimodal distribution is then accepted.

Monte Carlo simulations

The model is a system containing N_v vesicles and M_p peptides in a solution of total external volume V_t containing a dye at a concentration C_o per unit of volume equal to the vesicle lumen, V_o. The external solution reservoir (V_t) is assumed to be so large that C_o outside does not change when dye enters the vesicles. The membrane (surface) of each vesicle is divided into S peptide binding sites, with each site corresponding to L_s lipids. Typically, $S = 10^3$, $N_v = 100$, $M_p = 10000$, $L_s = 10$, and $V_t = 10^{10}$. The nominal ratios $[L] = N_v S L_s / V_t = 10^{-4}$ and $[P] = M_p / V_t = 10^{-6}$ correspond to initial concentrations of $[L] = 100$ μM lipid and $[P] = 1$ μM peptide. At low peptide concentrations on the membrane, L_s is essentially determined by the peptide length, whereas at higher concentrations the peptides tend to align because of Onsager ordering (36). The peptides are uniformly distributed in the external solution at time zero (as in the experiment). They bind to the vesicles with an on-rate constant k_{on}, set to 10^7 $M^{-1}s^{-1}$ per mole of binding sites (assuming $L_s = 10$ lipids, this corresponds to $k_{on} = 10^6$ $M^{-1}s^{-1}$ per mol-lipid). Peptides dissociate from the vesicles with an off-rate constant k_{off}, set to 10 s^{-1}. These values are fairly typical and yield an equilibrium dissociation constant $K_D = k_{off}/k_{on} = 1$ μM of binding sites, or 10 μM lipid, which is common for membrane-active peptides (3,6,7). When the peptide is bound to the vesicle surface, it can insert into the membrane, opening a pore, with a rate constant k_o. Here, by the term "pore", we simply mean that this peptide state allows dye influx to occur, with a flux rate constant k_x. The peptide returns to the surface, closing the pore, with a rate constant k_c.

Monte Carlo simulations are performed in this system as follows. A Monte Carlo cycle is defined as a number of attempted moves equal to the total number of sites in all vesicles, $N_v S$. To begin a cycle, a site on any vesicle is chosen at random. If the site is empty (no peptide bound or inserted), a peptide from solution can bind with probability $p_{bind} = k_{on}[P]\Delta\tau/S$, where $\Delta\tau$ is a small time step, set to 1 s in these simulations. Now, as in all other cases, to decide whether or not to accept the move (binding), a random number R is drawn; the move is accepted if $p_{bind} \geq R$ and rejected otherwise (37). If a peptide is bound to the vesicle surface on that site, a random decision is made first on whether to attempt dissociation or insertion in the membrane. The probability of dissociation is $p_{diss} = k_{off}\Delta\tau/S$ and the probability of insertion is $p_{ins} = k_o\Delta\tau/S$. (Note: because dissociation is only attempted half of the times (insertion is attempted the other half), binding is also attempted only half of the times to keep the ratio $k_{on}[P]/k_{off} = p_{bind}/p_{diss} = [P]/K_D$.) Finally, if a peptide is inserted at the site chosen, forming a pore, one of two processes can occur, with the choice between the two again being random. The peptide can return to the surface-bound state, closing the pore, with probability $p_{surf} = k_c\Delta\tau/S$, or dye influx can occur through the open pore with probability $p_{flux} = k_x(C_oV_o - N_{in})\Delta\tau/S$, where N_{in} is the number of dye molecules inside the vesicle. (Note: division by S in defining all those probabilities is not essential. The same results would be obtained by using a time step $\Delta\tau$ that is $S\times$ smaller. However, these definitions are convenient because the rates do not depend on the size of the vesicles, as they would otherwise, since the number of attempted moves in a cycle is proportional to the number of binding sites.) These processes are repeated for the number of cycles required to reach dye equilibrium across the vesicle membranes. The dye content of each vesicle is monitored as a function of time (number of cycles) and histograms of the distributions of vesicles according to their dye content are generated for comparison with those obtained experimentally.

RESULTS AND DISCUSSION

Peptide-induced influx in GUVs

In a typical confocal fluorescence microscopy experiment, POPC GUVs prepared in 0.1 M sucrose are added to a solution containing 50 μM CF, 1 μM peptide, and 0.1 M glucose in a glass culture dish. The sucrose solution is denser than the glucose solution, so the GUVs sink to the bottom of the glass dish and are observed with an inverted microscope. To aid in vesicle visualization, a lipid fluorophore, LRh-DOPE, is incorporated in the membrane (at 0.1 mol% of the POPC). As the peptides interact with the GUVs, CF influx occurs; the vesicle lumen, which initially is dark, progressively becomes greener, reflecting CF emission inside. An example is shown in Fig. 2 *A*, with influx induced by DL-1. The influx process can also be observed by differential interference contrast (Fig. 2 *B*) because the refraction index of the sucrose solution inside the vesicles is larger than that of the glucose solution outside (18,25,38). Typically, smooth dye influx caused by the peptides is observed, as shown for δ-lysin (Fig. 2 *C*) and DL-1 (*D*), but other processes are occasionally observed for the same peptides in the same samples. For example, vesicles may exhibit marked membrane undulations and deformations before influx occurs, or the GUV bursts or crumbles to a lipid blob. These events have also been reported by other investigators for other peptides and small compounds (39–44).

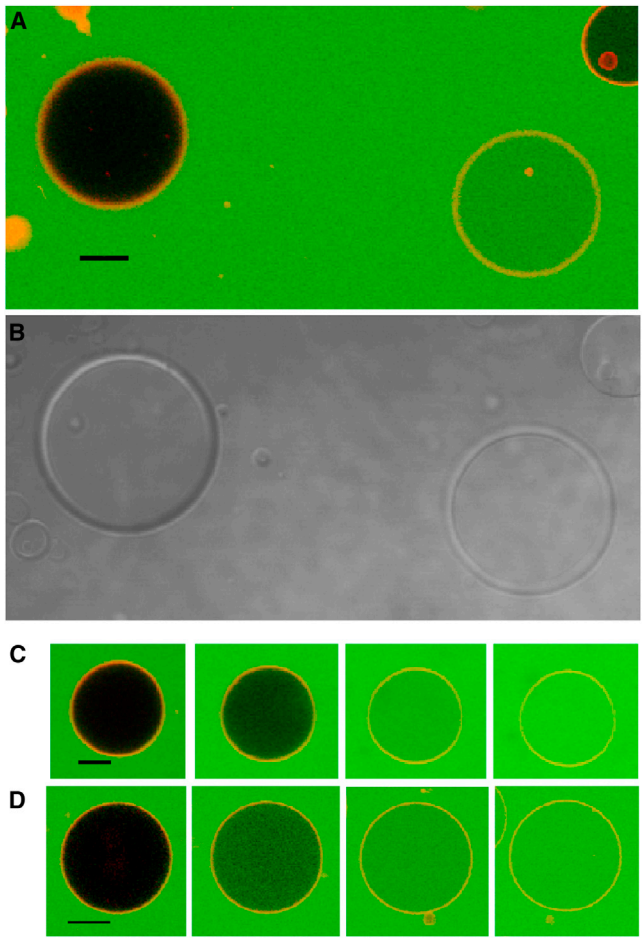

FIGURE 2 Confocal images of POPC GUVs containing 0.1 mol% LRh-DOPE prepared in 0.1 M sucrose, after addition to a solution containing $\sim$ 1 μM peptide, 50 μM CF, and 0.1 M glucose. (*A*) With DL-1, fluorescence mode, showing CF in green and LRh-DOPE in red. The left vesicle is almost empty and the right vesicle is almost full of CF; scale bar: 20 μm. (*B*) The same image in differential interference contrast mode. This also reflects the degree of filling because the refraction indexes of glucose and sucrose (internal, in left vesicle) are different. (*C*) Sequence of CF influx induced by δ-lysin. Images were taken at 5, 8, 13, and 16 min; scale bar: 10 μm. (*D*) Influx induced by DL-1. Images were taken at 32, 51, 58, and 99 min; scale bar: 20 μm.

Typically, the experiments lasted $\approx$ 1 h. In controls without peptides, performed for up to 3 h, <1% of the GUVs showed influx.

We wanted to determine whether the classification of peptides as graded or all-or-none in GUVs concurred with that obtained by the ANTS/DPX dye requenching assay in LUVs. The question is pertinent for two reasons: Both types of membranes are relatively unstrained, but GUVs have diameters $d \approx$ 10–100 μm, whereas LUVs are much smaller, $d \approx 0.1$ μm. The stability and curvature of the two membranes are quite different. More important, if the flux type is a property of the peptide, it should reflect the mechanism of its interaction with the membrane more than the type of vesicle. Note that we measure influx of dye into

GUVs but efflux from LUVs (dye release). This difference, however, is immaterial for the type of flux. We are aware of only one comparison, previously made for one peptide (mastoparan X), of the type of efflux in LUVs and small unilamellar vesicles (SUVs, $d \approx 30$ nm). Flux was graded in LUVs but close to all-or-none in SUVs (45). These vesicles, however, are extremely small and strained, and thus their interactions with peptides are likely to be very different from those of unstrained vesicles such as LUVs and GUVs.

Ideally, if dye flux is all-or-none, a GUV population in the middle of the process will consist of empty and full vesicles, whereas if the flux is graded, the sample will consist of vesicles with degrees of filling close to one-half (3). Fig. 3 shows examples of GUVs exposed to CE-2 (*A*) and DL-1 (*B*). In one case, the vesicles show intermediate degrees of filling (*A*), whereas in the other, they are either empty or full (*B*). This appears to correspond to graded and all-or-none fluxes. However, episodic observation of slow, continuous flux in a few vesicles is not sufficient to classify it as graded, and rapid flux in a few GUVs does guarantee all-or-none behavior. A more robust assessment is achieved by recording the degree of filling as a function of time for individual GUVs and comparing it with the average for the entire population (4,9). In graded flux, each vesicle should behave similarly to the entire population, whereas in all-or-none flux, individual vesicles should yield a series of influx steps as a function of time. Fig. 3 also shows this type of plot for GUVs exposed to CE-2 (*C*) and DL-1 (*D*). Here, the flux appears to be all-or-none in both cases. Typically, vesicles undergo influx either in one sharp step or continuously, but occasionally (<10 %) they exhibit more than one influx step. The onset of influx in each vesicle is stochastic.

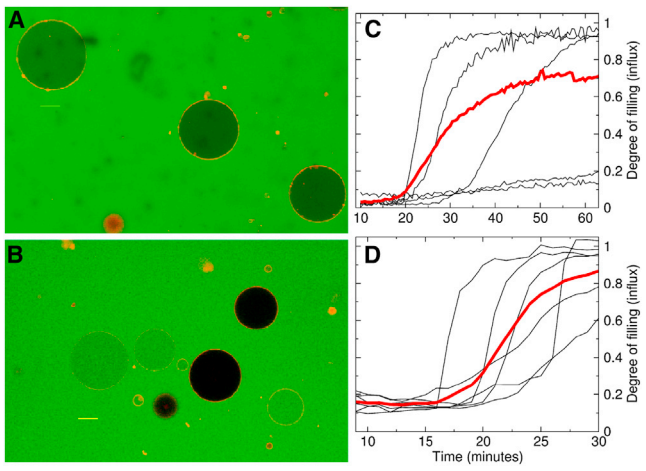

FIGURE 3 Left: POPC GUVs under the effect of (*A*) CE-2 and (*B*) DL-1. The lipid contains 0.1 mol% LRh-DOPE (*red*). Peptide: ~1 μM; CF (*green*): 50 μM; scale bar: 20 μm. Right: Degree of filling of POPC GUVs as a function of time upon addition to (*C*) CE-2 and (*D*) DL-1. The time is measured from the moment of addition of the GUVs to the peptide solution. Thin lines correspond to individual vesicles, and bold lines correspond to averages (seven vesicles for CE-2, and 51 for DL-1).

Inconsistencies arise if small numbers of vesicles are examined, because graded or all-or-none influx is a property of the vesicle distribution, not of individual vesicles. If the distribution of vesicles as a function of degree of filling is unimodal, influx is graded, and if the distribution is bimodal, influx is all-or-none. Those distributions are determined by the kinetics of pore opening and closing, and by the rate of flux through the pore, but the kinetics of individual or a few vesicles are not sufficient to establish the flux type.

Monte Carlo simulations of influx kinetics

To understand how different distributions of vesicle contents arise, we performed Monte Carlo simulations of influx kinetics in a very simple model that was stripped of all nonessential aspects, such as peptide oligomerization and translocation. We present the simulations first because this allows us to place the experimental distributions in the context of what is possible and expected. It also allows us to calibrate the statistical analysis of the distributions of degree of filling in the vesicles on very well defined cases.

The Monte Carlo simulations are performed on a large number of vesicles, which are initially empty, in a solution containing a fixed dye concentration. Peptides, uniformly distributed in this solution at time zero, are allowed to bind and dissociate from the vesicle surface, with rate constants k_{on} and k_{off}. When bound, the peptides can insert into the membrane, opening a pore, with rate constant k_o. Here, by the term "pore", we mean only that this peptide state allows dye influx to occur, but imply nothing about the pore structure. Any number of pores $\leq$ the number of peptides bound can exist in each vesicle. Influx of dye through the pore occurs with rate constant k_x. The peptide can return to the surface, closing the pore, with rate constant k_c.

In the simulations shown, 130 vesicles were used, because this is of the order of the number of vesicles examined experimentally (Table 1). The dye solution reservoir is assumed to be so large that its external concentration does not change when dye enters the vesicles. The numbers of vesicles and peptides were chosen to yield concentrations of lipid (130 μM) and peptide (1 μM) similar to those typically used in experiments. Lipid concentrations of 50–200 μM are common in LUV experiments. In GUVs, it is not possible to determine the lipid concentration exactly, but based on the vesicle density in microscope images, we estimate it to be $\sim$30–100 μM. We use $k_{off} = 10\ s^{-1}$ and $k_{on} = 10^7\ M^{-1}s^{-1}$ per binding site, which corresponds to $k_{on} = 10^6\ M^{-1}s^{-1}$ per lipid, since we assume $L_s = 10$ lipids per binding site. This yields an equilibrium dissociation constant $K_D = 10\ \mu$M lipid, which is typical for many membrane-active peptides (3,6,7).

We are not aware of experimental measurements of k_o, k_c, or k_x for membrane-active peptides. Therefore, in the simulations, k_o and k_c were varied between 10^{-3} and $10\ s^{-1}$ at

TABLE 1 Statistics of vesicle distributions in experiments and simulations

Peptide	Fig. 7		Dip	*p*-Value	Distribution	Flux type	No. of vesicles
Larger GUVs							
CE-2[a]	*A*		0.0701	3.7×10^{-4}	bimodal	all-or-none	107
DL-1[b]	*B*		0.0693	3.0×10^{-5}	bimodal	all-or-none	138
δ-Lysin[c]	*C*		0.0425	0.529	unimodal[d]	weakly graded	65
TPW-3[e]	*D*		0.0964	2.3×10^{-6}	bimodal	all-or-none	83
Smaller GUVs							
CE-2	*E*		0.0238	0.813	unimodal	graded	157
TPW-3	*F*		0.0489	0.08355	bimodal[f]	all-or-none	98
Simulation							
Figs. 4 and 6	k_o (s^{-1})	k_c (s^{-1})					
A	10^{-3}	10^{-1}	0.2031	$<2.2 \times 10^{-16}$	bimodal	all-or-none	130
B	10^{-3}	10	0.0221	0.960	unimodal	graded	130
C	1.0	1.0	0.0199	0.990	unimodal	graded	130
D	10^{-2}	10^{-3}	0.1138	$<2.2 \times 10^{-16}$	bimodal	all-or-none	130
E	3×10^{-2}	10^{-3}	0.0654	2.2×10^{-4}	bimodal	all-or-none	130
F	10^{-1}	10^{-3}	0.0189	0.992	unimodal	graded	130

[a]KWKLLKKLEKAGAALKEGLLKAGPALALLGAAAALAK-amide.
[b]formyl-MAQKIISTIGKLVKWIIKTVNKFTKK.
[c]formyl-MAQDIISTIGDLVKWIIDTVNKFTKK.
[d]See text for details.
[e]AGWLLGDINLKALAALAKKIL-amide.
[f]The statistics indicate borderline bimodal. See text for discussion.

fixed k_x. For reference, we estimated k_x from permeability measurements of ions through small pores and pure bilayers. The membrane permeability (P) is related to the dye flux rate constant by $k_x = 3P/r$ (46–48), where r is the radius of a spherical vesicle. Since the permeability of a pure fluid bilayer to ions is $P \sim 10^{-11}$ cm s^{-1} (46), $k_x \approx 10^{-6}$ to 10^{-5} s^{-1}. Ion permeability through a small but well-defined pore is estimated as $P \sim 10^{-2}$ cm s^{-1} (49), which is ~9 orders of magnitude faster, so $k_x \approx 10^3$ s^{-1}. The flux rate through a membrane perturbed by a peptide must lie between these two extremes, and the values used fall within this range ($k_x = 1$, 0.1, and 0.01 s^{-1}).

In each set of simulations, the flux rate (k_x) was fixed and the other rate constants were varied. Their magnitudes are meaningful only in comparison with k_x. Varying the on- and off-rates (k_{on} and k_{off}) over two orders of magnitude had a negligible effect on the flux kinetics. This is because the binding equilibrium is reached much faster than the subsequent bilayer perturbation. On the other hand, varying the rate constants of pore opening and closing, k_o and k_c, had a profound effect on whether dye flux was graded or all-or-none.

Distributions of vesicles in the simulations

The distributions of vesicles as a function of their degree of filling were recorded in the Monte Carlo simulations. A representative set is shown in Fig. 4 at the midpoint of influx, that is, when the average degree of filling in the ensemble in each simulation is 0.50. Each panel shows the histogram and the probability density function (curve) of the distribution. The density function was calculated directly from the raw data (degree of filling of each vesicle), using the statistically optimal bandwidth. Like the histogram, the density function provides a visual idea of the modality of the distribution, but does not depend on the choice of bin size in the histogram. However, to rigorously determine whether a distribution is unimodal or bimodal, we performed the standard test for modality, Hartigan's dip test (22). The smaller the value of the dip statistic (D), the higher is the probability that the distribution is unimodal. The distributions obtained from the Monte Carlo simulations provide a calibration and allow us to build an intuition for the meaning of Hartigan's dip test. This understanding will be used in the analysis of the experimental results. The dip values and the corresponding p-values for the distributions obtained in the simulations are listed in Table 1.

The distributions shown in Fig. 4 were obtained with an influx rate $k_x = 1$ s^{-1}. Their differences arise solely from varying k_o and k_c, with all other rate constants fixed. An extreme bimodal distribution, the hallmark of all-or-none flux, is shown in Fig. 4 *A*, where $k_o = 10^{-3}$ and $k_c = 10^{-1}$ s^{-1}, both $\ll k_x$. The dip value is $D = 0.2031$ and $p < 2.2 \times 10^{-16}$ (Table 1). These are the largest D-values and smallest p-values we can expect in such systems. A clear unimodal distribution, characteristic of graded flux, is shown in Fig. 4 *B*, obtained with the same $k_o = 10^{-3}$ s^{-1} but with a much larger rate of pore closing, $k_c = 10$ s^{-1}. Here $D = 0.0221$ (10× smaller than in A) and $p = 0.960$, close to the theoretical maximum (1.0), clearly indicating that the distribution is unimodal. Another unimodal distribution is shown in Fig. 4 *C*, obtained with $k_o = k_c = 1$ $s^{-1} = k_x$. The dip is $D = 0.0199$ and $p = 0.960$, almost the same as in Fig. 4 *B*.

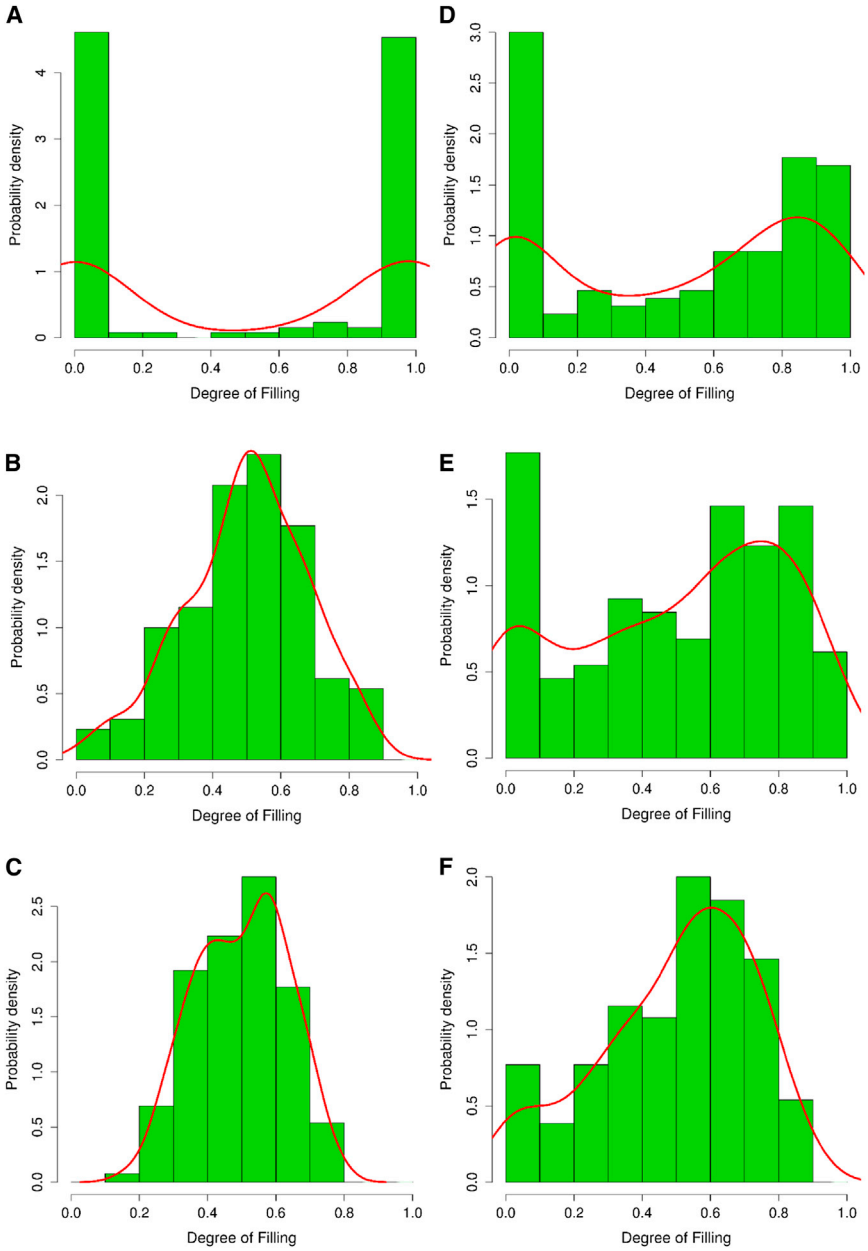

FIGURE 4 Histograms and probability density functions (curves) of the distributions of degree of filling of vesicles calculated from Monte Carlo simulations, varying the rate constants for pore opening (k_o) and closing (k_c) at fixed $k_x = 1\ s^{-1}$. (*A*) all-or-none, $k_o = 10^{-3}$, $k_c = 10^{-1}\ s^{-1}$; (*B*) graded, $k_o = 10^{-3}$, $k_c = 10\ s^{-1}$; (*C*) graded, $k_o = 1$, $k_c = 1\ s^{-1}$. (*D*) all-or-none, $k_o = 10^{-2}$, $k_c = 10^{-3}\ s^{-1}$; (*E*) all-or-none, $k_o = 3 \times 10^{-2}$, $k_c = 10^{-3}\ s^{-1}$; (*F*) graded, $k_o = 10^{-1}$, $k_c = 10^{-3}\ s^{-1}$. The other rate constants are fixed at $k_{on} = 10^7\ M^{-1}s^{-1}$ per binding site and $k_{off} = 10\ s^{-1}$. Each distribution contains a total of 130 vesicles. For the histograms, density = (number of vesicles in bin)/(total number of vesicles per bin). For easy reference, the tallest bins in each panel correspond to the following numbers of vesicles: (*A*) 60, (*B*) 31, (*C*) 30, (*D*) 18, (*E*) 36, and (*F*) 26.

The series of panels in Fig. 4, *D–F*, show the change of a distribution from bimodal (all-or-none flux) to unimodal (graded), as the rate of pore opening increases from $k_o = 10^{-2}$ (*D*) to 3×10^{-2} (*E*) to $10^{-1}\ s^{-1}$ (*F*), with fixed $k_c = 10^{-3}\ s^{-1} \ll k_x$. Thus, changing k_o by a factor of 10, from *D* to *F*, changed the nature of the distribution completely. To our knowledge, this dependence of flux type on k_o has not been previously demonstrated.

A systematic variation of k_o and k_c reveals the general behavior of the system. Fig. 5 shows surface plots of the dip value (*A*) and $1-p$-value (*B*) for the distributions of degree of filling in the Monte Carlo simulations. We plot the $1-p$-value (Fig. 5 *B*) because it is easier to compare with the dip surface (Fig. 5 *A*; both are large for bimodal distributions and approach zero for unimodal distributions). On the top of the surface, if k_o and k_c are both very small ($\leq 10^{-2}\ s^{-1}$) compared with k_x ($1\ s^{-1}$), influx is all-or-none. As k_o or k_c increase, the surface falls off to graded influx at the base. Thus, if k_o increases to $1\ s^{-1}$, the flux becomes graded. But to obtain graded flux by changing k_c, it has to approach $10\ s^{-1}$. Thus, the transition is primarily influenced by how the opening rate k_o compares with k_x.

Schwarz and Robert (50) derived an analytical relation between the type of flux and the ratio of the rate of pore closing to dye flux, which applies if the measuring time in an experiment is much longer than the open pore lifetime ($\tau_o = 1/k_c$) and if pores form at a constant, slow rate $k_o \ll k_c$. Under these conditions, if $k_c \ll k_x$ (long-lived

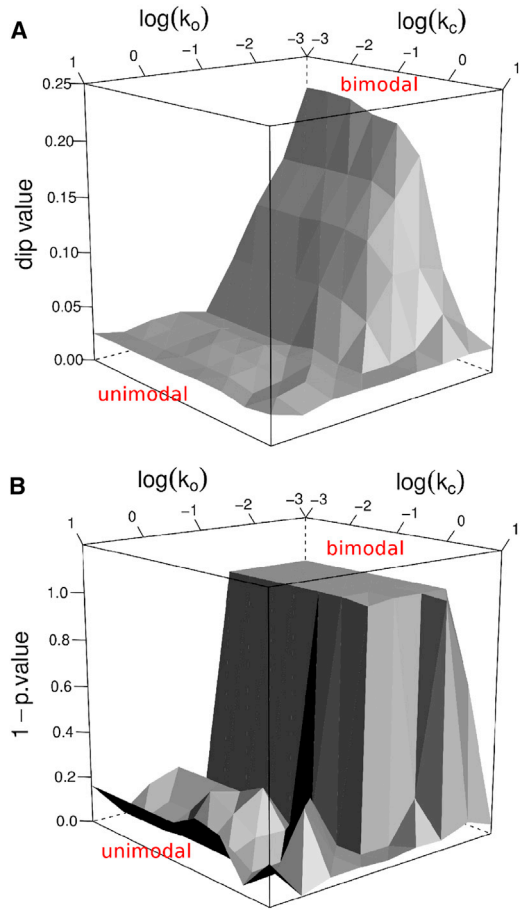

FIGURE 5 Effect of varying the opening and closing rates, k_o and k_c (logarithmic scale, base 10), with $k_x = 1\ s^{-1}$, on the modality of the distributions in Monte Carlo simulations. (*A*) Dip value. The base, close to $D = 0.02$ corresponds to unimodal distributions (graded flux), whereas $D = 0.2$ corresponds to strongly bimodal (all-or-none flux). (*B*) The associated *p*-value. A *p*-value close to 1.0 ($1-p \approx 0$) corresponds to a unimodal distribution (graded flux), whereas a *p*-value <0.05 ($1-p > 0.95$) corresponds to a bimodal distribution (all-or-none flux).

pores), dye flux is all-or-none. But if $k_c \gg k_x$ (short-lived pores), the flux is graded (50). These behaviors match the Monte Carlo simulation results if pores open slowly, $k_o \leq 10^{-2}\ s^{-1}$, with $k_x = 1\ s^{-1}$. However, it is actually easier to obtain graded flux by increasing k_o with small k_c than the converse. It was previously pointed out that the opening rate affects the type of flux (3), but here we present the first (to our knowledge) quantitative demonstration of this effect.

Finally, if $k_x = 0.1\ s^{-1}$, the all-or-none region will shrink significantly. And if $k_x = 10^{-2}\ s^{-1}$, even the case $k_o = k_c = 10^{-3}\ s^{-1}$ will become graded. It is a curious observation that the symmetry of the type of dye flux with respect to interchange of k_o and k_c in the Monte Carlo simulations (Fig. 5 *A*) is reminiscent of a well-known property of the probability that a pore is in the open state if the open and closed time intervals are random (51).

Fig. 6 shows plots of influx as a function of time in the simulations. The panels correspond exactly to those in Fig. 4. The bold line represents the average degree of filling in the simulation sample, and each thin line represents an individual vesicle. Fig. 6 *A* shows the archetypal all-or-none case, in which each vesicle undergoes influx stochastically and rapidly, at a rate much different from that of the overall process. Fig. 6 *C* shows the archetypal graded case, in which all vesicles undergo influx at approximately the same rate, very similar to the overall influx in the sample. In Figure 6 *B*, some vesicles undergo bursts of influx at very different rates from the average, but the overall process is graded. Fig. 6, *D–F*, show the transition from all-or-none to graded flux, as the opening rate constant increases from 10^{-2} to $10^{-1}\ s^{-1}$. In these panels, it is not as straightforward to assign the nature of the influx based solely on the influx kinetics, but the distributions need to be analyzed (Fig. 4, *D–F*; Table 1).

Experimental Distributions of GUVs and graded or all-or-none influx

We are now ready to analyze the experimental distributions of GUVs as a function of dye influx induced by the various

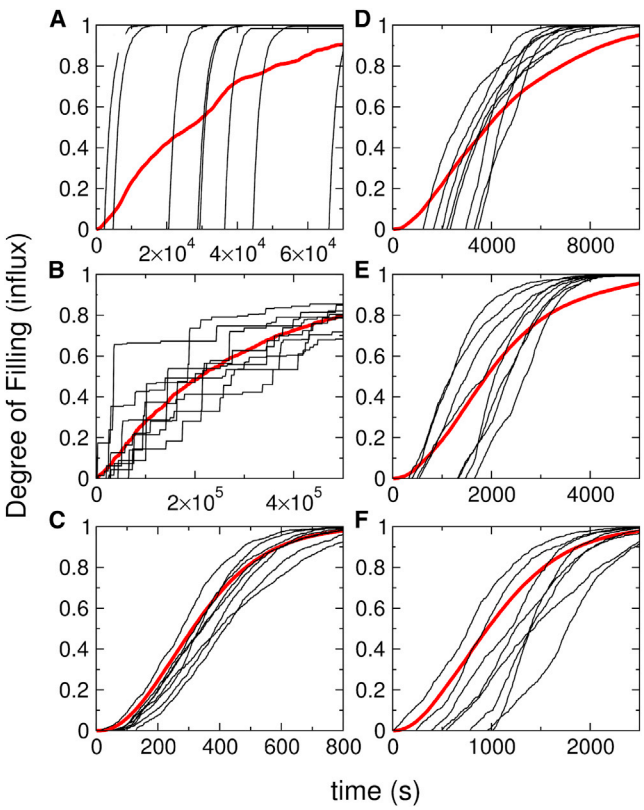

FIGURE 6 Examples of degree of filling of vesicles as a function of time in Monte Carlo simulations. The thin lines represent individual vesicles. The bold line represents averages of 130 vesicles. The panels correspond to the same exact simulations as in Fig. 4.

peptides. The flux induced by the four peptides now investigated in GUVs was previously determined in LUVs (6,7,21) using the ANTS/DPX requenching assay (Fig. 1). To facilitate comparison between the two experiments, it is important to convey the gist of the ANTS/DPX assay (13–15). The fluorophore (ANTS) and the quencher (DPX) are both encapsulated in the vesicles (LUVs). When the peptides interact with the membrane, ANTS leaks out of the vesicles (as does DPX, at a comparable rate), but is requenched by external, newly added DPX. Thus, only the fluorescence arising from inside the vesicles is measured. In graded release, the fluorescence coming from inside the vesicles rises gradually, as shown in Fig. 1 for CE-2 (*A*) and δ-lysin (*C*), because the quencher concentration decreases as efflux progresses. In all-or-none release, only the intact vesicles contribute to the observed fluorescence, and the degree of quenching inside those vesicles is independent of the amount released by the others. Therefore, the plot of the fluorescence inside as a function of ANTS released is a horizontal line, as shown in Fig. 1 *B* for DL-1.

To unambiguously determine the flux type in GUVs, we examined the distribution of vesicles as a function of their degree of dye filling. The histograms and probability density functions (curves) of these distributions are shown in Fig. 7 at the midpoint of the influx process, that is, when the average degree of filling in the sample is ≈ 0.50. The results of the statistical analysis of these distributions are listed in Table 1. Vesicles that were obviously defective or paucilamellar were excluded, but vesicles that eventually burst were included if they were intact at the midpoint of influx. For comparison, note that if LUVs were to burst, they would become invisible in the ANTS/DPX assay (because the externally added DPX quenches the released fluorophore). Thus, the criteria are the same in both experiments.

In Fig. 7, *A–D*, we focus on the larger GUVs in the population to make the most dramatic comparison with LUVs ($d \approx 0.1$ μm). Thus, only GUVs with $d > 15$ μm are included in these distributions. In Fig. 7, *E* and *F*, we examine the distributions of the smaller GUVs in the population, with $d < 15$ μm. By inspection of the histograms, the GUV dye content distribution appears bimodal for CE-2 (*A*), DL-1 (*B*), and TPW-3 (*D*), but the situation is unclear for δ-lysin (*C*). To put these assignments on a rigorous basis, we calculated the density function of the distributions and performed the Hartigan dip test for modality (22), as in the simulations. Consider first the larger GUVs ($d > 15$ μm). In the case of CE-2, the distribution is clearly bimodal (Fig. 7 *A*). The dip test returns $D = 0.0701$ and $p = 3.7 \times 10^{-4}$ (Table 1), which is a measure of how likely this distribution could arise by chance, assuming that the null hypothesis is true (unimodal distribution). Bimodal distributions are also obtained with DL-1 (*B*), with $D = 0.0693$ and $p = 3.0 \times 10^{-5}$, and even more clearly with TPW-3 (*D*), with $D = 0.0964$ and $p = 2.3 \times 10^{-6}$. The situation is less evident for δ-lysin (*C*). The histogram appears unimodal, even though a large bar occurs at complete filling, but the density function is essentially unimodal with a high shoulder (Fig. 7 *C*). The dip test yields $D = 0.0425$, which is very close to the base of the surface plot of the dip value (Fig. 5 *A*), indicating a unimodal distribution. The p-value$= 0.529$, which is clearly not small enough to discard the unimodal distribution. Now consider the smaller GUVs ($d < 15$ μm). With CE-2, the distribution is clearly unimodal (Fig. 7 *E*). The dip test yields $D = 0.0238$, close to the lowest dips observed in simulations, and $p = 0.813$, which is sufficiently close to 1.0 (Table 1). With TPW-3, the situation is less clear in the smaller GUVs (Fig. 7 *F*). The distribution appears bimodal, as in large GUVs; however, the dip is only $D = 0.0489$ and $p = 0.0835 > 0.05$, so the unimodal distribution cannot be discarded with the same confidence.

Finally, let us compare the results obtained in GUVs (Fig. 7) with those previously obtained in LUVs using the ANTS/DPX assay (Fig. 1). In the case of DL-1 (Figs. 1 *B* and 7 *B*), the flux was all-or-none in both assays (7). For TPW-3 (Figs. 1 *D* and 7 *D*), the flux had been deemed weakly graded (6). However, that assignment perhaps weighed the data point at the highest amount of release too heavily (Fig. 1 *D*); without that point, the ANTS/DPX assay indicates all-or-none flux. Now we find that the distribution of degree of filling is bimodal in larger GUVs, and probably also in the smaller ones, indicating that TPW-3 causes all-or-none flux. The situation with δ-lysin (Fig. 1 *C*) is less clear. In GUVs it appears to induce graded influx, but the statistics are not as conclusive. In LUVs, with the ANTS/DPX assay, a classification as weakly graded appears appropriate (21), and is corroborated by the results presented here. Finally, CE-2 produced the most interesting (and surprising) results. In LUVs, (Fig. 1 *A*) this peptide induces clearly graded flux (7). The same is observed in the smaller GUVs (Fig. 7 *E*), but in the larger GUVs the flux is all-or-none (Fig. 7 *A*). Thus, in this case, the flux type changes with the vesicle size.

CONCLUSIONS

In this work, we compared dye flux induced by four membrane-active peptides (CE-2, DL-1, δ-lysin, and TPW-3) in LUVs and GUVs. For three of these peptides, the type of flux is the same in both types of vesicles. The exception is CE-2, which causes graded flux in LUVs and smaller GUVs, but all-or-none flux in the largest GUVs. Thus, the type of flux does not necessarily reflect a fundamental mechanism by which peptides permeabilize membranes.

In addition, we compared the experimental results with those of Monte Carlo simulations of dye influx using a very simple model, which gave us a deeper understanding of graded and all-or-none fluxes across membranes, and of the factors that determine them. Fundamentally, the nature of graded or all-or-none flux is statistical, not kinetic. If the distribution of vesicles as a function of degree of filling

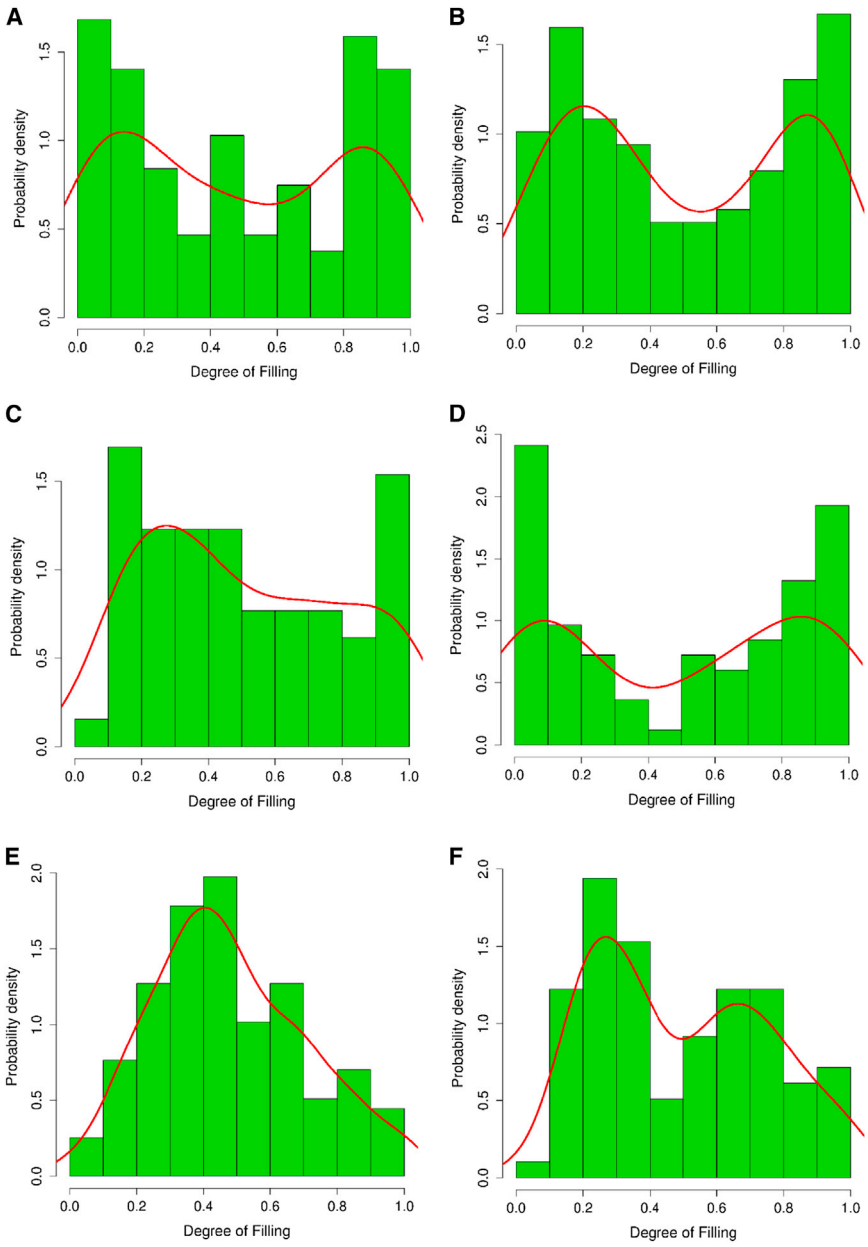

FIGURE 7 Histograms and probability density functions (curves) of the distributions of degree of filling of POPC GUVs in the presence of each peptide at the influx midpoint. Larger GUVs: (*A*) CE-2, (*B*) DL-1, (*C*) δ-lysin, and (*D*) TPW-3. Smaller GUVs: (*E*) CE-2, (*F*) TPW-3. For the histograms, density = (number of vesicles in bin)/(total number of vesicles per bin). For easy reference, the tallest bins in each panel correspond to the following numbers of vesicles: (*A*) 18, (*B*) 18, (*C*) 12, (*D*) 20, (*E*) 31, and (*F*) 19. The total numbers of GUVs in each distribution are indicated in Table 1; they were recorded in 5 independent samples for CE-2, 9 for DL-1, 6 for δ-lysin, and 4 for TPW-3.

is unimodal, influx is graded, and if the distribution is bimodal, influx is all-or-none. These distributions arise from different kinetics, but the kinetics of individual or a few vesicles are not sufficient to establish the flux type.

If the opening and closing rates remain constant, as the movement of solutes through a pore becomes slower, the influx becomes graded. In experiments, this occurs because slower influx corresponds to smaller pores. What is less intuitive is that increasing the rate of pore opening, for fixed rates of pore closing and flux through the pore, results in graded flux (Fig. 5). What happens is that the overall influx becomes much faster, but all vesicles have degrees of filling similar to the overall average, which means that flux is graded.

Almeida and Pokorny (1) conjectured that the two types of flux indicate whether peptides translocate across the membrane or not. The idea is that peptide translocation depends on its propensity to insert into the lipid bilayer. The Gibbs free energy of insertion (ΔG_{ins}) was estimated using the experimental free energy of binding and approximating the transfer to the bilayer interior by transfer to octanol (52). The hypothesis is that if $\Delta G_{ins} \leq 20$ kcal/mol, the peptide is able to translocate, but if $\Delta G_{ins} > 23$ kcal/mol, it is not (1). Further, it was observed that δ-lysin, mastoparans, melittin, and variants of the cell-penetrating peptide TP10 caused graded dye flux (1,6,53), whereas the antimicrobial peptides cecropin A and magainin 2 caused all-or-none flux (8–12). Since the peptides that caused

graded flux had $\Delta G_{ins} \leq 20$ kcal/mol, it was proposed that graded flux indicates the peptide propensity to translocate across the membrane. It is now evident, however, that there is no general relation between ΔG_{ins} and the flux type. The peptide CE-2, which is a variant of cecropin A, has $\Delta G_{ins} = 36$ kcal/mol (7); it should not translocate and should cause all-or-none flux. However, CE-2 causes graded flux in LUVs and in the smaller GUVs, but all-or-none flux in the largest GUVs. It is unlikely that the mechanism of its interaction with the membrane changes from smaller to larger GUVs. Furthermore, for TPW-3, $\Delta G_{ins} = 17$ kcal/mol (6), but release is all-or-none, at least in GUVs. Whether or not there is a relation between ΔG_{ins} and peptide translocation across the bilayer is a question that remains to be resolved.

We thank Dr. Antje Pokorny for many discussions, and Dr. Ana García-Sáez for her generous advice on various technical aspects of GUV preparation and the confocal microscopy experiments. We are very grateful to Dr. Richard Dillaman and Mark Gay for their support in the use of the confocal fluorescence microscope at the UNCW Microscopy Facility. Finally, we acknowledge Dr. Susan Simmons for her advice on statistical analysis with R.

This work was supported by National Institutes of Health grant GM072507. The UNCW Microscopy Facility is funded by National Science Foundation grant DBI 0420948.

REFERENCES

1. Almeida, P. F., and A. Pokorny. 2009. Mechanisms of antimicrobial, cytolytic, and cell-penetrating peptides: from kinetics to thermodynamics. *Biochemistry.* 48:8083–8093.
2. Wimley, W. C. 2010. Describing the mechanism of antimicrobial peptide action with the interfacial activity model. *ACS Chem. Biol.* 5:905–917.
3. Almeida, P. F., and A. Pokorny. 2012. Interactions of antimicrobial peptides with lipid bilayers. *In* Comprehensive Biophysics. E. H. Egelman, editor. Membranes, Vol. 5. L. Tamm, editor. Academic Press, Oxford. 189–222.
4. Fuertes, G., A. J. García-Sáez, …, J. Salgado. 2010. Pores formed by Baxα5 relax to a smaller size and keep at equilibrium. *Biophys. J.* 99:2917–2925.
5. Tamba, Y., H. Ariyama, …, M. Yamazaki. 2010. Kinetic pathway of antimicrobial peptide magainin 2-induced pore formation in lipid membranes. *J. Phys. Chem. B.* 114:12018–12026.
6. McKeown, A. N., J. L. Naro, …, P. F. Almeida. 2011. A thermodynamic approach to the mechanism of cell-penetrating peptides in model membranes. *Biochemistry.* 50:654–662.
7. Clark, K. S., J. A. Svetlovics, …, P. F. Almeida. 2011. What determines the activity of antimicrobial and cytolytic peptides in model membranes. *Biochemistry.* 50:7919–7932.
8. Gregory, S. M., A. Pokorny, and P. F. F. Almeida. 2009. Magainin 2 revisited: a test of the quantitative model for the all-or-none permeabilization of phospholipid vesicles. *Biophys. J.* 96:116–131.
9. Tamba, Y., and M. Yamazaki. 2005. Single giant unilamellar vesicle method reveals effect of antimicrobial peptide magainin 2 on membrane permeability. *Biochemistry.* 44:15823–15833.
10. Tamba, Y., and M. Yamazaki. 2009. Magainin 2-induced pore formation in the lipid membranes depends on its concentration in the membrane interface. *J. Phys. Chem. B.* 113:4846–4852.
11. Gregory, S. M., A. C. Cavenaugh, …, P. F. F. Almeida. 2008. A quantitative model for the all-or-none permeabilization of phospholipid vesicles by the antimicrobial peptide cecropin A. *Biophys. J.* 94:1667–1680.
12. Silvestro, L., K. Gupta, …, P. H. Axelsen. 1997. The concentration-dependent membrane activity of cecropin A. *Biochemistry.* 36:11452–11460.
13. Wimley, W. C., M. E. Selsted, and S. H. White. 1994. Interactions between human defensins and lipid bilayers: evidence for formation of multimeric pores. *Protein Sci.* 3:1362–1373.
14. Ladokhin, A. S., W. C. Wimley, and S. H. White. 1995. Leakage of membrane vesicle contents: determination of mechanism using fluorescence requenching. *Biophys. J.* 69:1964–1971.
15. Ladokhin, A. S., W. C. Wimley, …, S. H. White. 1997. Mechanism of leakage of contents of membrane vesicles determined by fluorescence requenching. *Methods Enzymol.* 278:474–486.
16. Apellániz, B., J. L. Nieva, …, A. J. García-Sáez. 2010. All-or-none versus graded: single-vesicle analysis reveals lipid composition effects on membrane permeabilization. *Biophys. J.* 99:3619–3628.
17. Lee, M.-T., W.-C. Hung, …, H. W. Huang. 2008. Mechanism and kinetics of pore formation in membranes by water-soluble amphipathic peptides. *Proc. Natl. Acad. Sci. USA.* 105:5087–5092.
18. Mally, M., J. Majhenc, …, B. Žekš. 2007. The response of giant phospholipid vesicles to pore-forming peptide melittin. *Biochim. Biophys. Acta.* 1768:1179–1189.
19. Kokot, G., M. Mally, and S. Svetina. 2012. The dynamics of melittin-induced membrane permeability. *Eur. Biophys. J.* 41:461–474.
20. Yandek, L. E., A. Pokorny, …, P. F. F. Almeida. 2007. Mechanism of the cell-penetrating peptide transportan 10 permeation of lipid bilayers. *Biophys. J.* 92:2434–2444.
21. Pokorny, A., and P. F. F. Almeida. 2004. Kinetics of dye efflux and lipid flip-flop induced by δ-lysin in phosphatidylcholine vesicles and the mechanism of graded release by amphipathic, α-helical peptides. *Biochemistry.* 43:8846–8857.
22. Hartigan, J. A., and P. M. Hartigan. 1985. The dip test of unimodality. *Ann. Stat.* 13:70–84.
23. Angelova, M. I., S. Soléau, …, P. Bothorel. 1992. Preparation of giant vesicles by external AC electric fields. Kinetics and applications. *Prog. Colloid Polym. Sci.* 89:127–131.
24. Reeves, J. P., and R. M. Dowben. 1969. Formation and properties of thin-walled phospholipid vesicles. *J. Cell. Physiol.* 73:49–60.
25. Akashi, K., H. Miyata, …, K. Kinosita, Jr. 1996. Preparation of giant liposomes in physiological conditions and their characterization under an optical microscope. *Biophys. J.* 71:3242–3250.
26. Akashi, K., H. Miyata, …, K. Kinosita, Jr. 1998. Formation of giant liposomes promoted by divalent cations: critical role of electrostatic repulsion. *Biophys. J.* 74:2973–2982.
27. Morales-Penningston, N. F., J. Wu, …, G. W. Feigenson. 2010. GUV preparation and imaging: minimizing artifacts. *Biochim. Biophys. Acta.* 1798:1324–1332.
28. Moscho, A., O. Orwar, …, R. N. Zare. 1996. Rapid preparation of giant unilamellar vesicles. *Proc. Natl. Acad. Sci. USA.* 93:11443–11447.
29. Svetlovics, J. A., S. A. Wheaten, and P. F. Almeida. 2012. Phase separation and fluctuations in mixtures of a saturated and an unsaturated phospholipid. *Biophys. J.* 102:2526–2535.
30. Collins, T. J. 2007. ImageJ for microscopy. *Biotechniques.* 43(1, Suppl):25–30.
31. Bevington, P. R., and D. K. Robinson. 1992. Data Reduction and Error Analysis for the Physical Sciences. McGraw-Hill, New York.
32. Sturges, H. A. 1926. The choice of a class interval. *J. Am. Stat. Assoc.* 21:65–66.
33. R Project for Statistical Computing. R: a language and environment for statistical computing. http://www.R-project.org. Accessed 2013.
34. Priebe, N. J., F. Mechler, …, D. Ferster. 2004. The contribution of spike threshold to the dichotomy of cortical simple and complex cells. *Nat. Neurosci.* 7:1113–1122.

35. Mechler, F., and D. L. Ringach. 2002. On the classification of simple and complex cells. *Vision Res.* 42:1017–1033.

36. Almeida, P. F. F., and F. W. Wiegel. 2006. A simple theory of peptide interactions on a membrane surface: excluded volume and entropic order. *J. Theor. Biol.* 238:269–278.

37. Metropolis, N., A. W. Rosenbluth, …, E. Teller. 1953. Equation of state calculations by fast computing machines. *J. Chem. Phys.* 21:1087–1092.

38. Yunus, W. M. M., and A. B. Rahman. 1988. Refractive index of solutions at high concentrations. *Appl. Opt.* 27:3341–3343.

39. Domingues, T. M., K. A. Riske, and A. Miranda. 2010. Revealing the lytic mechanism of the antimicrobial peptide gomesin by observing giant unilamellar vesicles. *Langmuir.* 26:11077–11084.

40. Yu, Y., J. A. Vroman, …, S. Granick. 2010. Vesicle budding induced by a pore-forming peptide. *J. Am. Chem. Soc.* 132:195–201.

41. Tamba, Y., S. Ohba, …, M. Yamazaki. 2007. Single GUV method reveals interaction of tea catechin (-)-epigallocatechin gallate with lipid membranes. *Biophys. J.* 92:3178–3194.

42. Cabrera, M. P., D. S. Alvares, …, J. R. Neto. 2011. New insight into the mechanism of action of wasp mastoparan peptides: lytic activity and clustering observed with giant vesicles. *Langmuir.* 27:10805–10813.

43. Semrau, S., M. W. L. Monster, …, M. Overhand. 2010. Membrane lysis by gramicidin S visualized in red blood cells and giant vesicles. *Biochim. Biophys. Acta.* 1798:2033–2039.

44. Kristanc, L., S. Svetina, and G. Gomišček. 2012. Effects of the pore-forming agent nystatin on giant phospholipid vesicles. *Biochim. Biophys. Acta.* 1818:636–644.

45. Schwarz, G., and A. Arbuzova. 1995. Pore kinetics reflected in the dequenching of a lipid vesicle entrapped fluorescent dye. *Biochim. Biophys. Acta.* 1239:51–57.

46. Paula, S., A. G. Volkov, …, D. W. Deamer. 1996. Permeation of protons, potassium ions, and small polar molecules through phospholipid bilayers as a function of membrane thickness. *Biophys. J.* 70:339–348.

47. Faure, C., F. Nallet, …, O. Lambert. 2006. Modeling leakage kinetics from multilamellar vesicles for membrane permeability determination: application to glucose. *Biophys. J.* 91:4340–4349.

48. Verkman, A. S., J. A. Dix, and J. L. Seifter. 1985. Water and urea transport in renal microvillus membrane vesicles. *Am. J. Physiol.* 248:650–655.

49. Bolintineanu, D., E. Hazrati, …, Y. N. Kaznessis. 2010. Antimicrobial mechanism of pore-forming protegrin peptides: 100 pores to kill *E. coli*. *Peptides.* 31:1–8.

50. Schwarz, G., and C. H. Robert. 1992. Kinetics of pore-mediated release of marker molecules from liposomes or cells. *Biophys. Chem.* 42:291–296.

51. Colquhoun, D., and A. G. Hawkes. 1994. The interpretation of single channel recordings. *In* Microelectrode Techniques, The Plymouth Workshop Handbook, 2nd ed. D. Ogden, editor. Company of Biologists Ltd., Cambridge, UK. 141–188.

52. Wimley, W. C., T. P. Creamer, and S. H. White. 1996. Solvation energies of amino acid side chains and backbone in a family of host-guest pentapeptides. *Biochemistry.* 35:5109–5124.

53. Rex, S., and G. Schwarz. 1998. Quantitative studies on the melittin-induced leakage mechanism of lipid vesicles. *Biochemistry.* 37:2336–2345.